Supporting Information

Multi-Site Functional Cathode Interlayers for High-Performance Binary Organic Solar Cells

Zhihui Chen,‡[a] Qi Li,‡[a] Yufeng Jiang,[b] Hyunbok Lee,[c] Thomas P. Russell,[b, d] and Yao Liu*[a]

[a] State Key Laboratory of Chemical Resource Engineering, Beijing Advanced Innovation Center for Soft Matter Science and Engineering, Beijing University of Chemical Technology, Beijing 100029, China

[b] Polymer Science and Engineering Department, University of Massachusetts Amherst, 120 Governors Drive, Amherst, Massachusetts 01003, United States

[c] Department of Physics, Kangwon National University, 1 Gangwondaehak-gil, Chuncheon-si, Gangwon-do 24341, Republic of Korea

[d] Materials Sciences Division, Lawrence Berkeley National Lab, 1 Cyclotron Road, Berkeley, California 94720, United States

1. Material Characterizations

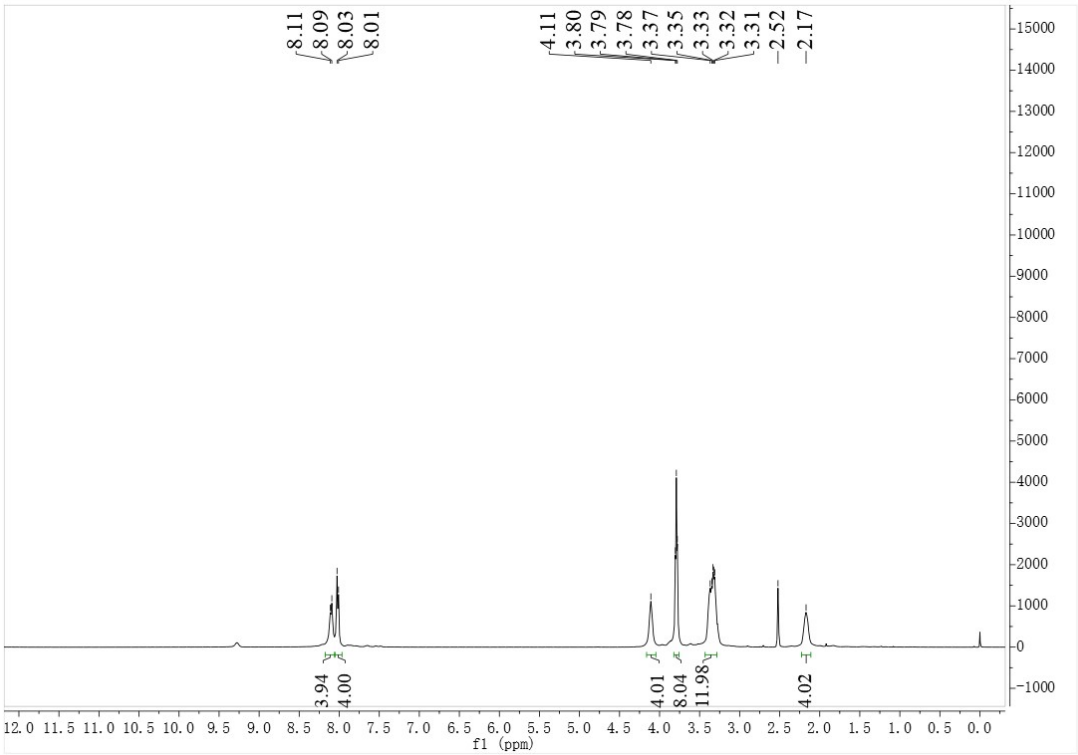

Figure S1. ^{1}H NMR spectrum of PDI-EA.

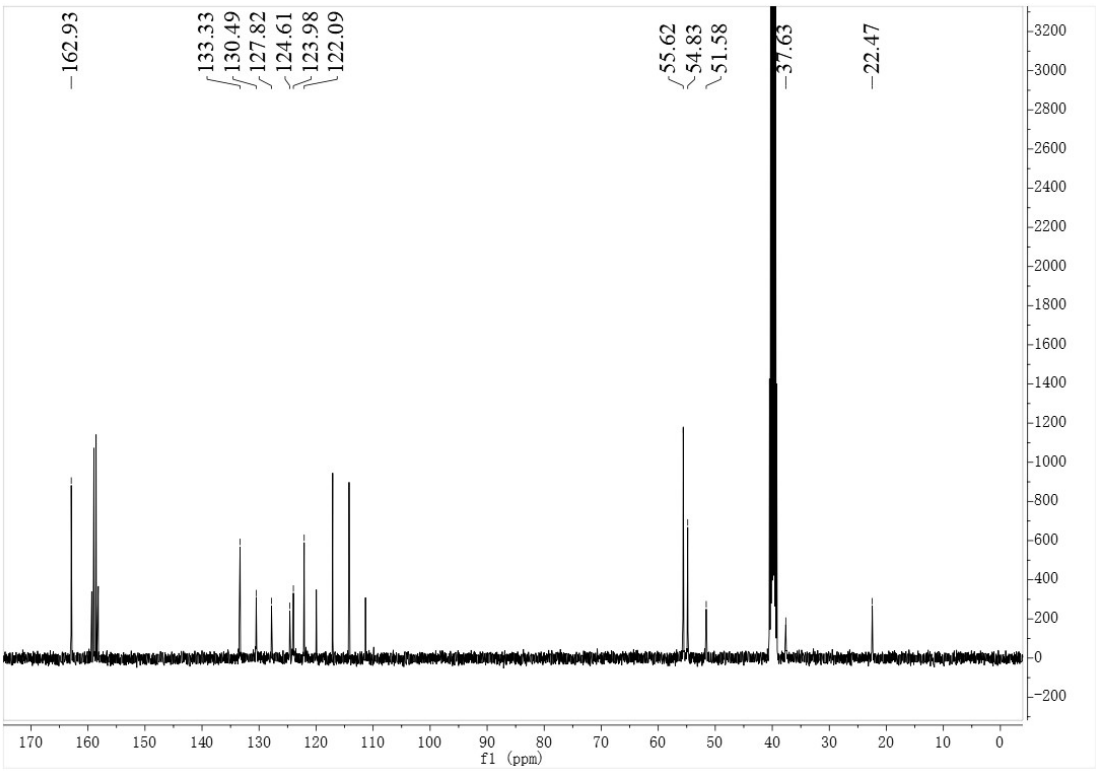

Figure S2. ^{13}C NMR spectrum of PDI-EA.

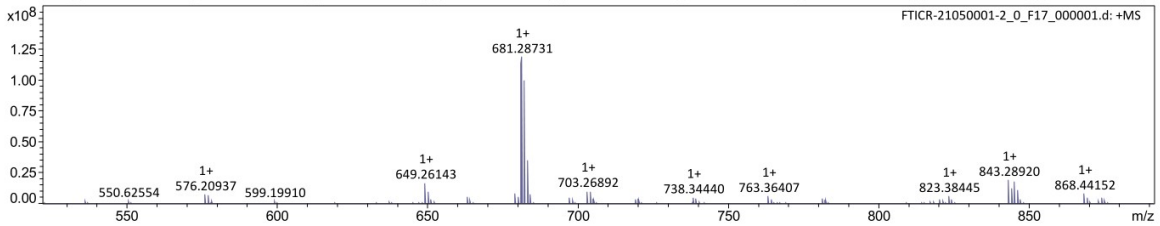

Figure S3. MALDI-TOF mass spectrometry of PDI-EA.=

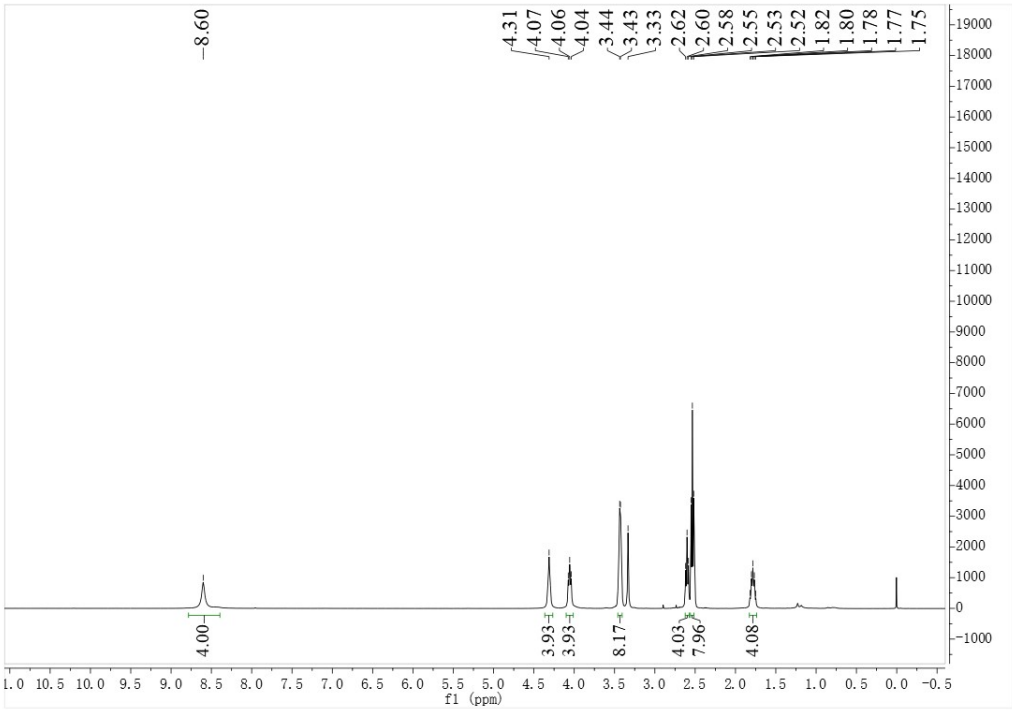

Figure S4. ^{1}H NMR spectrum of NDI-EA

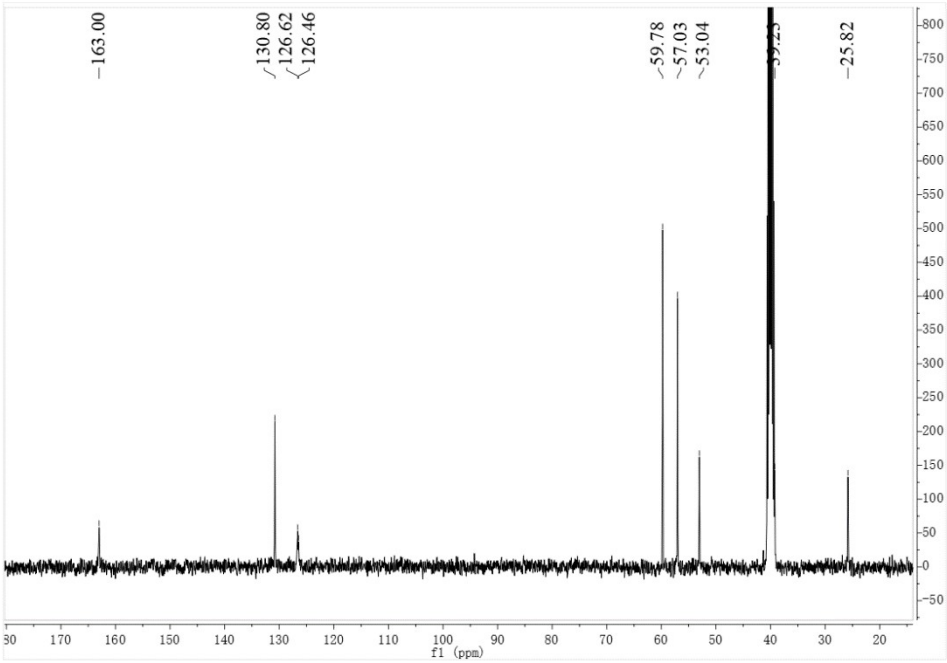

Figure S5. ^{13}C NMR spectrum of PDI-EA

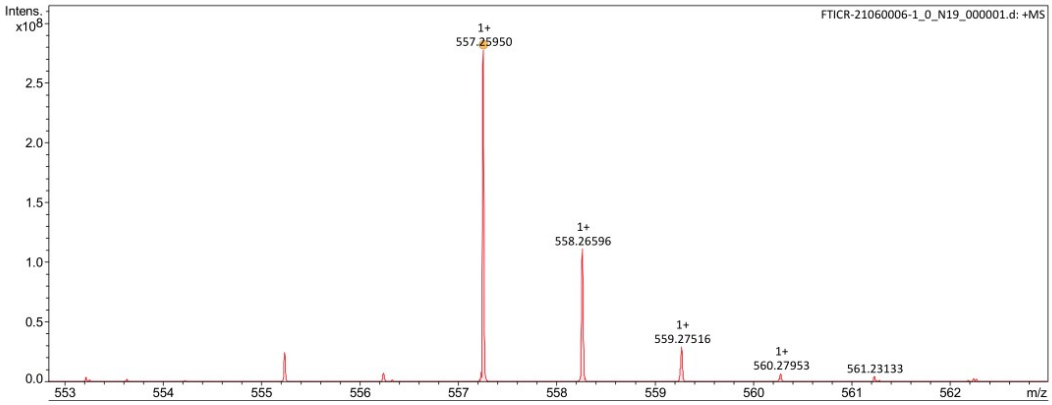

Figure S6. MALDI-TOF mass spectrometry of PDI-EA.

Table S1. The evaluated cost for chemical synthesis of PDI-EA.

Materials	Price (RMB)	Brand	Price of PDI-EA ($)
3,4,9,10-perylenetetracarboxylic dianhydride	312/100 g	MREDA	$2.75/g
N-(3-aminopropyl) diethanolamine	6072/500 g	TCI	
N,*N*-dimethylformamide , 99.8%, Super dry	207/L	J&K	
Methanol	50/L	J&K	

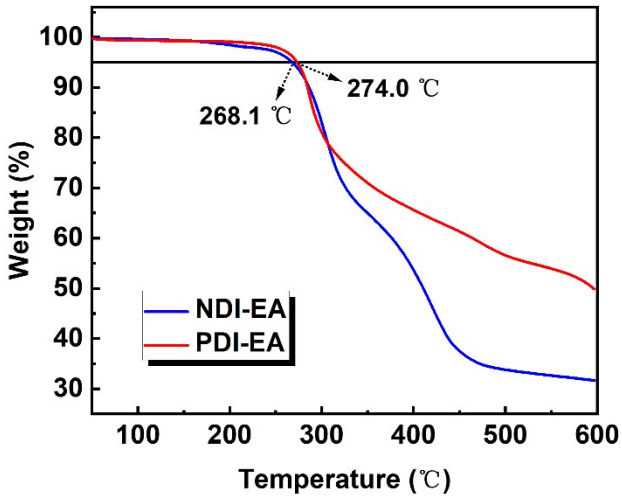

Figure S7. TGA plots of NDI-EA and PDI-EA.

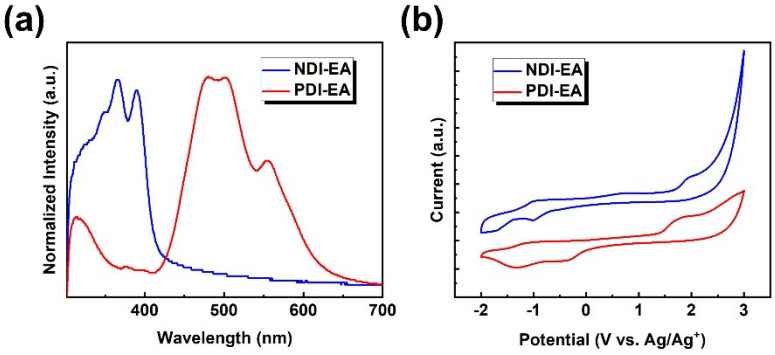

Figure S8. a) Normalized UV-vis spectra of PDI-EA and NDI-EA thin films. b) Cyclic voltammetry analyses of PDI-EA and NDI-EA.

Table S2. Summaries of optical and energetical properties based on PDI-EA and NDI-EA thin films.

Interlayer materials	Film absorption (nm)		E_g^{opt} [eV] [a)]	LUMO [eV] [b)]	HOMO [eV] [b)]	EA [eV] [c)]	IP [eV] [c)]
	λ_{max}	λ_{edg}					
NDI-EA	389	415	2.99	−3.65	−6.29	3.32	6.31
PDI-EA	480	632	1.96	−4.03	−6.05	4.03	5.99

[a)] Calculated from optical absorption edges: $E_g^{opt} = 1240 / \lambda_{edg}$; [b)] Calculated from CV: $E_{HOMO/LUMO} = -(E_{onset}^{ox/red} + 4.80 - E_{onset,\ Fc/Fc^+})$; [c)] Calculated from UPS measurements: $IP = h\nu - (E_{cutoff} - E_{H,\ onset})$

2. Device characterizations

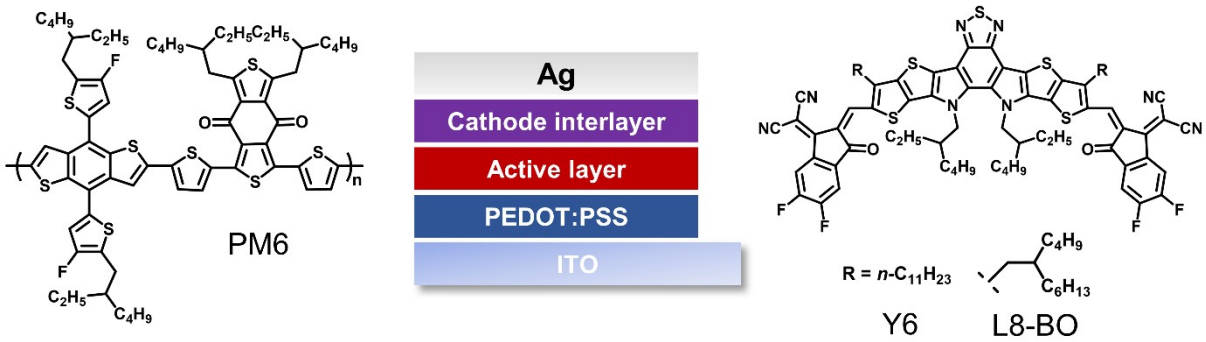

Figure S9. Schematic device configuration and chemical structures of PM6, Y6 and L8-BO involved in this work.

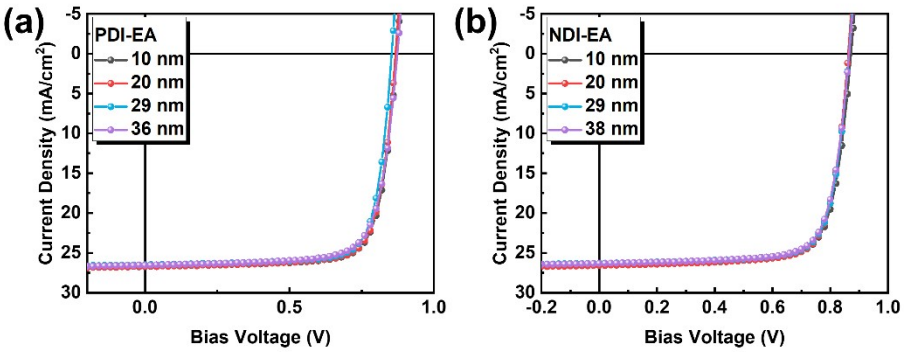

Figure S10. Thickness dependency of photovoltaic performances for a) PDI-EA and b) NDI-EA based OSCs.

Table S3. Summary of the recently recorded efficiencies in OSCs with different cathode interlayers.

Interlayer material	Solar cell structure	PCE_{max}(%)	Ref.
PDI-EA	ITO/PEDOT:PSS/PM6:Y6/CIL/Ag	18.04	This work
PDI-EA	ITO/PEDOT:PSS/PM6:L8-BO/CIL/Ag	18.50	This work
NDI-NI	ITO/PEDOT:PSS/PM6:Y6/CIL/Ag	16.27	1
PDINN	ITO/PEDOT:PSS/PM6:Y6/CIL/Ag	17.23	2
PDI-M	ITO/PEDOT:PSS/PM6:Y6/CIL/Ag	17.65	3
SiNcTI-Br	ITO/PEDOT:PSS/PM6:Y6/CIM/Ag	16.71	4
SME1	ITO/PEDOT:PSS/PM6:Y6/CIL/Ag	17.5	5
PBI-2P	ITO/PEDOT:PSS/PM6:BTP-eC9/CIL/Ag	18.4	6
CTOC-N-Br	ITO/PEDOT:PSS/PM6:BTP-4Cl/CIL/Ag	17.19	7
HBC-S	ITO/PEDOT:PSS/PM6:BTP-eC9/CIL/Ag	18.05	8
PNDIT-F3N-Br	ITO/PEDOT:PSS/PM6:L8-BO/CIL/Ag	18.32	9

Table S4. Summary of photovoltaic performance based on devices PM6: Y6 prepared with NDI-EA and PDI-EA at different thicknesses. The average performances are shown in parenthetically and calculated from at least ten devices.

Interlayer materials	Thickness (nm)	V_{OC} (V)	*FF* (%)	J_{SC} (mA/cm^2)	*PCE* (%)
PDI-EA	10	0.87 (0.87 ± 0.01)	77.70 (77.61 ± 0.19)	26.69 (26.65 ± 0.13)	18.04 (17.99 ± 0.03)
	20	0.86 (0.87 ± 0.01)	77.57 (77.38 ± 0.02)	26.70 (26.68 ± 0.07)	17.93 (17.91 ± 0.02)
	29	0.85 (0.86 ± 0.01)	77.99 (77.15 ± 0.81)	26.49 (26.62 ± 0.13)	17.61 (17.62 ± 0.06)
	36	0.87 (0.86 ± 0.01)	75.49 (75.40 ± 0.51)	26.54 (26.66 ± 0.27)	17.47 (17.40 ± 0.05)
NDI-EA	10	0.87 (0.87 ± 0.01)	76.75 (76.56 ± 0.30)	26.36 (26.45 ± 0.08)	17.62 (17.58 ± 0.05)
	20	0.86 (0.86 ± 0.01)	76.73 (76.44 ± 0.34)	26.58 (26.53 ± 0.07)	17.56 (17.51 ± 0.04)
	29	0.86 (0.86 ± 0.01)	76.60 (76.26 ± 0.29)	26.30 (26.31 ± 0.08)	17.39 (17.28 ± 0.10)
	38	0.86 (0.86 ± 0.01)	75.97 (75.86 ± 0.37)	26.33 (26.25 ± 0.06)	17.28 (17.18 ± 0.12)

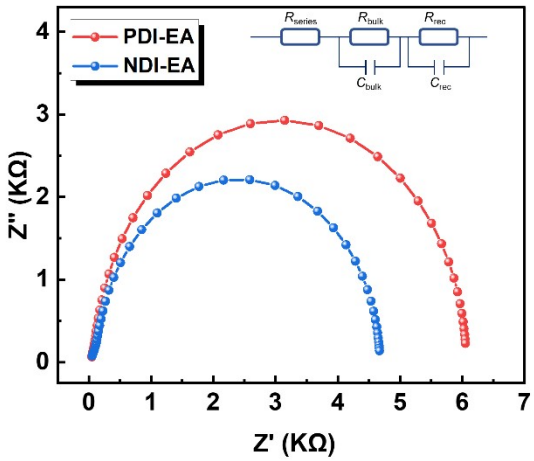

Figure S11. Nyquist plot of PDI-EA and NDI-EA modified devices and the equivalent-circuit model.

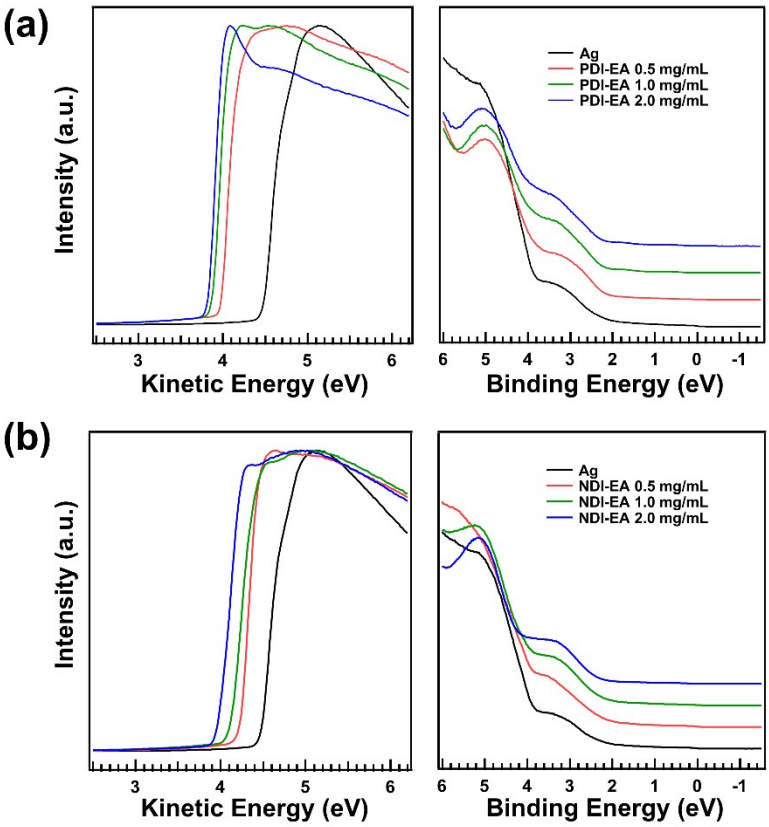

Figure S12.UPS spectra of bare Ag, PDI-EA and NDI-EA at different concentrations.

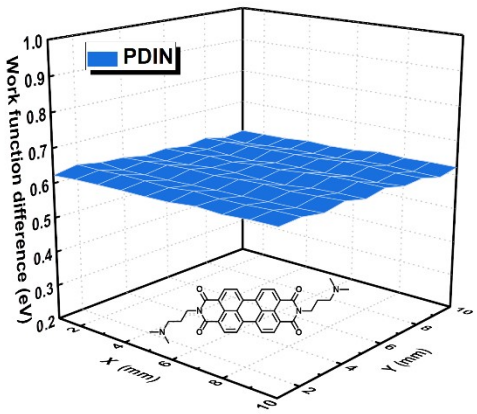

Figure S13. Work function reduction of Ag/PDIN and molecular structure of PDIN.

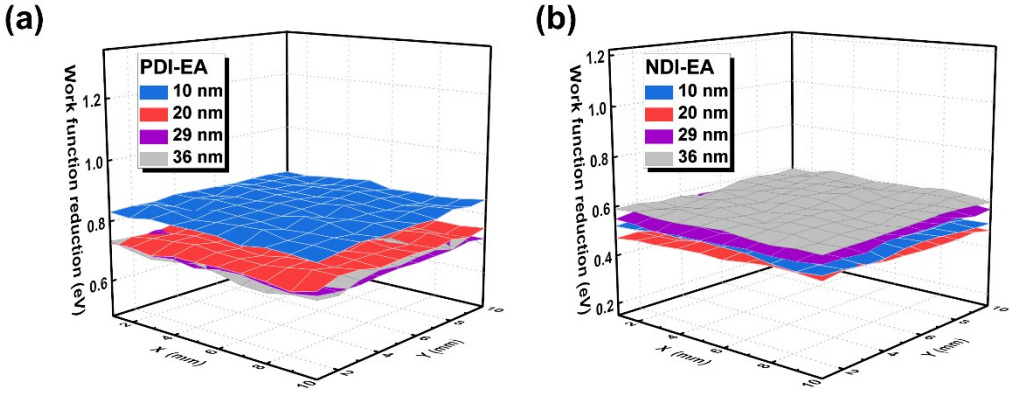

Figure S14. Thickness dependency of work function reductions for a) PDI-EA and b) NDI-EA modified Ag surfaces.

Table S5. Summaries of work function differences of Ag surfaces after modification by PDI-EA and NDI-EA with different thicknesses.

Interlayer materials	10 nm	20 nm	29 nm	36-38 nm
NDI-EA	0.52 ± 0.01	0.48 ± 0.01	0.56 ± 0.01	0.60 ± 0.01
PDI-EA	0.84 ± 0.01	0.74 ± 0.01	0.72 ± 0.01	0.72 ± 0.01

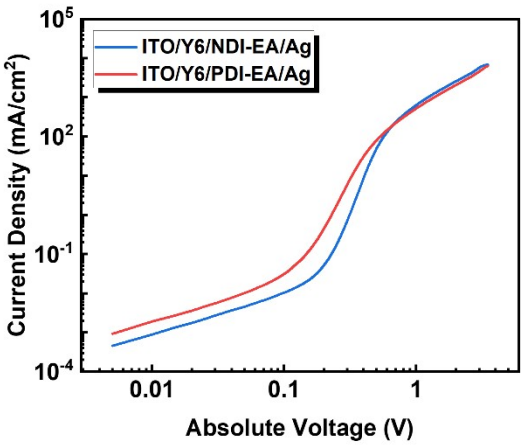

Figure S15. Space charge limited current plots of PDI-EA and NDI-EA based electron-only devices.

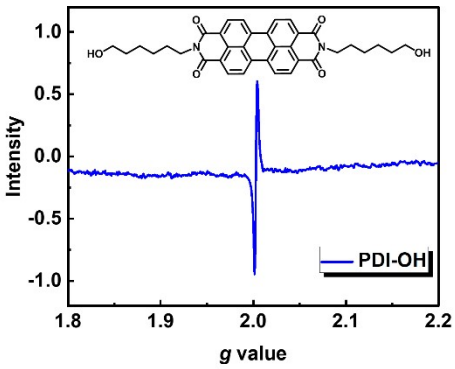

Figure S16. ESR signals for PDI-OH with inset of molecular structure of PDI-OH.

Table S6. The comparison between PDINO and PDI-EA.

Interlayer materials	LUMO(eV)	HOMO(eV)	Conductivity (S cm^{-1})	Work function of Ag (eV)	PM6:Y6 based OSC efficiency (%)
PDI-EA	-4.03	-6.05	8.4×10^{-3}	3.82	18.04
PDINO	-3.63	-6.21	7.6×10^{-5}	3.88	15.17

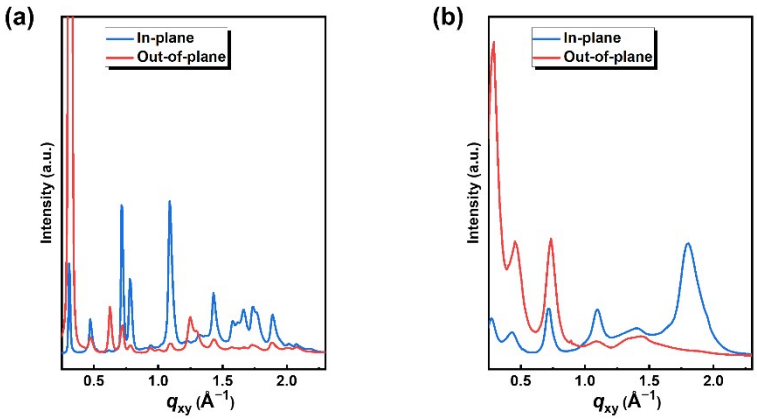

Figure S17. GIXD 1D line cuts for a) NDI-EA and b) PDI-EA thin films.

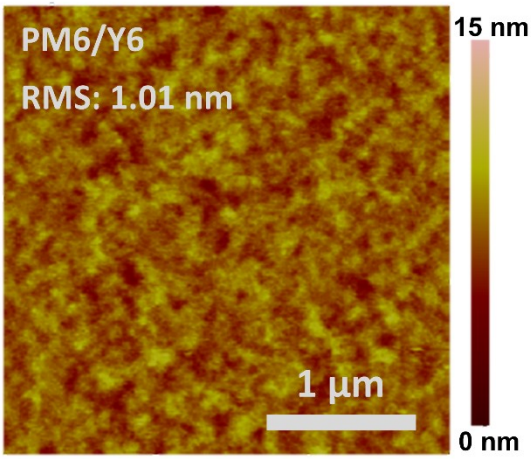

Figure S18. AFM images for neat PM6:Y6 surface morphologies.

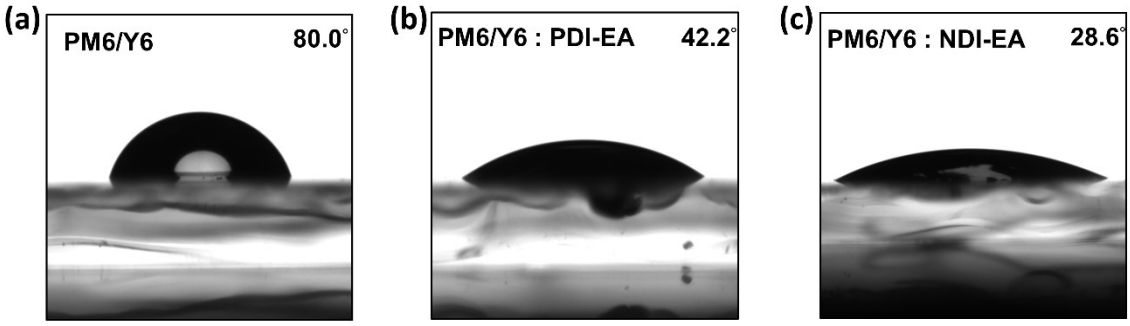

Figure S19. Contact angle images of a) neat PM6:Y6, b) PM6:Y6 modified by PDI-EA, and c) PM6:Y6 modified by NDI-EA with the water droplet on top.

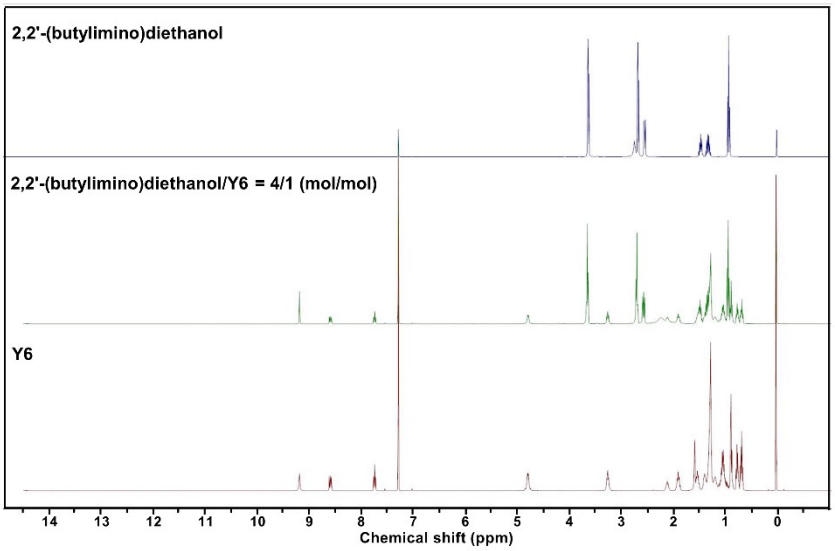

Figure S20. ^{1}H NMR spectra of neat 2,2'-(butylimino)diethanol, 2,2'-(butylimino)diethanol /Y6 blends, and neat Y6.

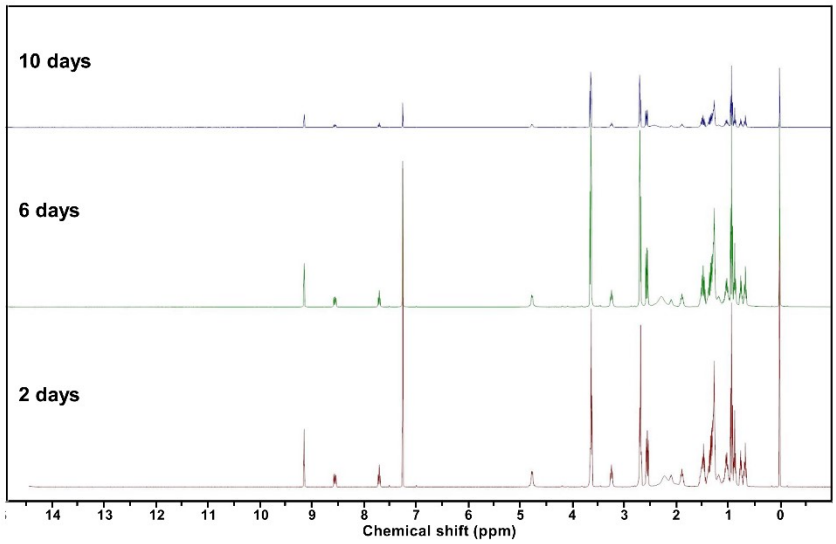

Figure S21. ^{1}H NMR spectra of 2,2'-(butylimino)diethanol/Y6 blends on the different days.

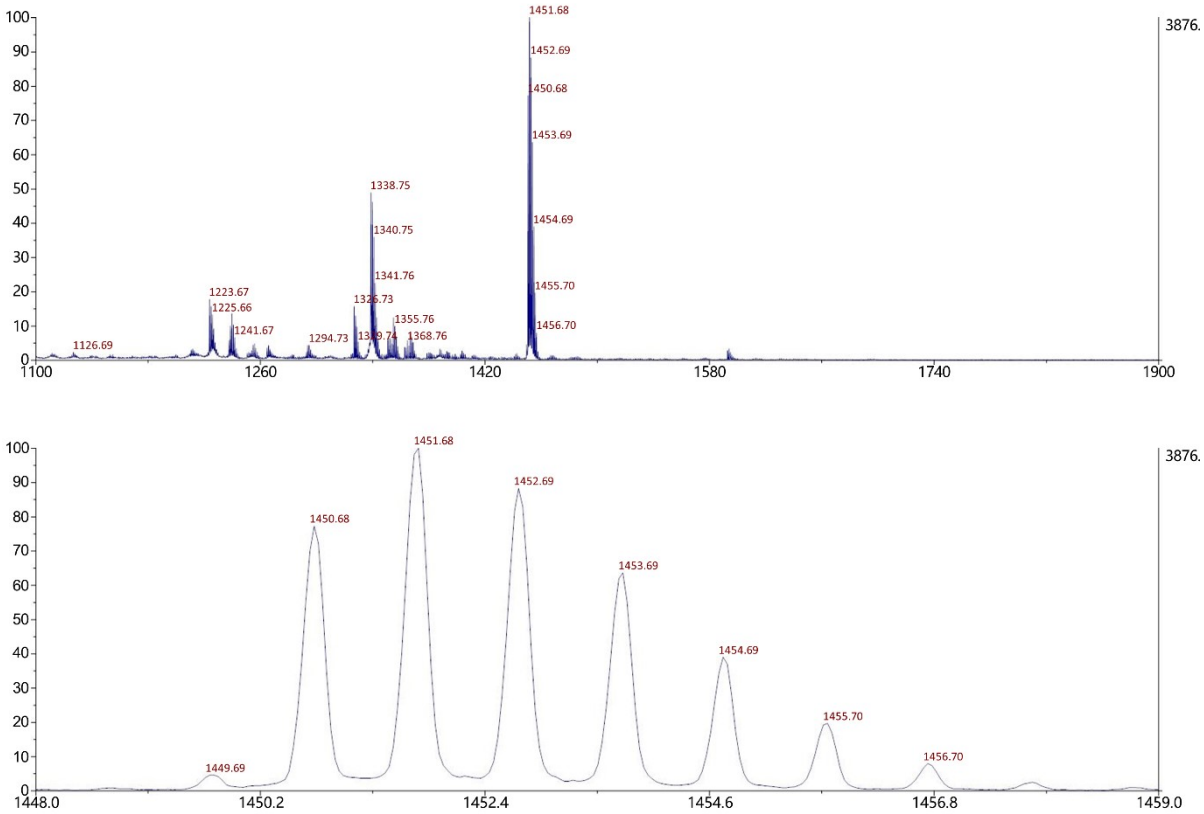

Figure S22. MALDI-TOF mass spectrometry of 2,2'-(butylimino)diethanol/Y6 blends (4/1 mol/mol) on the 10th day.

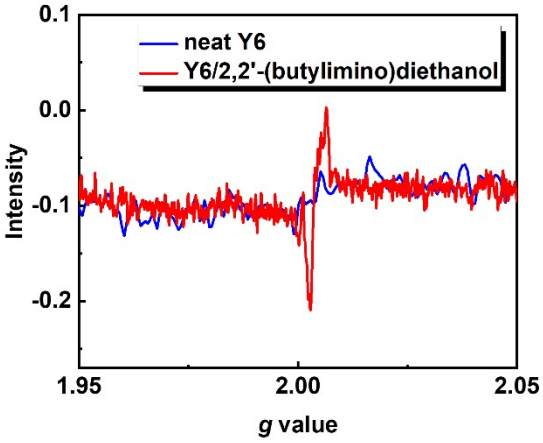

Figure S23. ESR profiles for neat Y6 and 2,2'-(butylimino)diethanol/Y6 (1/1 *w*/*w*) blends.

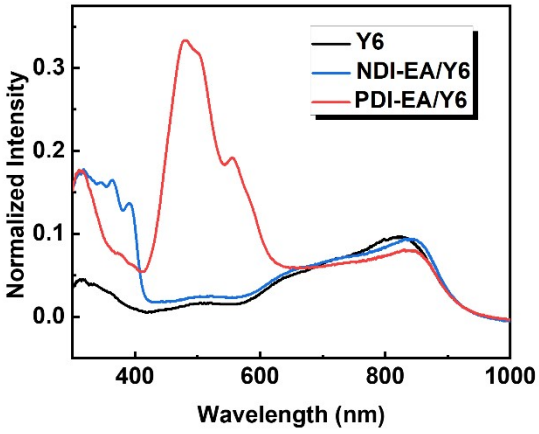

Figure S24. UV-vis spectra for neat Y6, NDI-EA coated on Y6, and PDI-EA coated on Y6 thin films.

References

1 M. Liu, P. Fan, Q. Hu, T. P. Russell and Y. Liu, Angew. Chem. Int. Ed., 2020, 59, 18131-18135.

2 J. Yao, B. Qiu, Z. G. Zhang, L. Xue, R. Wang, C. Zhang, S. Chen, Q. Zhou, C. Sun, C. Yang, M. Xiao, L. Meng and Y. Li, Nat. Commun., 2020, 11, 1-10.

3 M. Liu, Y. Jiang, D. Liu, J. Wang, Z. Ren, T. P. Russell and Y. Liu, ACS Energy Lett., 2021, 6, 3228-3235.

4 C. Cai, J. Yao, L. Chen, Z. Yuan, Z. G. Zhang, Y. Hu, X. Zhao, Y. Zhang, Y. Chen and Y. Li, Angew. Chem. Int. Ed., 2021, 60, 19053-19057.

5 Y. Qin, Y. Chang, X. Zhu, X. Gu, L. Guo, Y. Zhang, Q. Wang, J. Zhang, X. Zhang, X. Liu, K. Lu, E. Zhou, Z. Wei and X. Sun, Nano Today, 2021, 41.

6 X. Wen, Y. Zhang, G. Xie, R. Rausch, N. Tang, N. Zheng, L. Liu, F. Würthner and Z. Xie, Adv. Funct. Mater., 2022, DOI: 10.1002/adfm.202111706, 2111706.

7 C. Zhao, Z. Zhang, F. Han, D. Xia, C. Xiao, J. Fang, Y. Zhang, B. Wu, S. You, Y. Wu and W. Li, Angew. Chem. Int. Ed., 2021, 60, 8526-8531.

8 L. Liu, S. Chen, Y. Qu, X. Gao, L. Han, Z. Lin, L. Yang, W. Wang, N. Zheng, Y. Liang, Y. Tan, H. Xia and F. He, Adv. Mater., 2021, 33, 2101279.

9 C. Li, J. Zhou, J. Song, J. Xu, H. Zhang, X. Zhang, J. Guo, L. Zhu, D. Wei, G. Han, J. Min, Y. Zhang, Z. Xie, Y. Yi, H. Yan, F. Gao, F. Liu and Y. Sun, Nat. Energy., 2021, 6, 605-613.